Magnetoplasmonic nanograting geometry enables optical nonreciprocity sign control

L. Halagačka, Mathias Vanwolleghem, Francois Vaurette, J. Ben Youssef, K. Postava, J. Pištora, Béatrice Dagens

Magnetoplasmonic nanograting enables optical nonreciprocity sign reversal

L. Halagačka,[1,*] M. Vanwolleghem,[2], F. Vaurette,[2]
J. Ben Youssef,[3] K. Postava,[1] J. Pištora,[1] and B. Dagens,[4,**]

[1] *IT4Innovations and Nanotechnology Centre, Technical University Ostrava, 708 33 Ostrava-Poruba, Czech Republic*
[2] *Institut d'Electronique, de Microélectronique et de Nanotechnologie, CNRS UMR 8520, Université Lille 1, 59652 Villeneuve d'Ascq Cedex, France*
[3] *Lab-STICC, UMR 6285/CNRS-Université de Bretagne Occidentale, 29285 Brest Cedex 3, France*
[4] *Centre de Nanosciences et de Nanotechnologies, CNRS, Univ. Paris-Sud, Université Paris-Saclay, C2N-Orsay, 91405 Orsay cedex, France*
[*] *lukas.halagacka@gmail.com*
[**] *beatrice.dagens@c2n.upsaclay.fr*

Abstract:

We experimentally demonstrate a disruptive approach to control magnetooptical nonreciprocal effects. It has been known that the combination of a magneto-optically (MO) active substrate and extraordinary transmission (EOT) effects through deep-subwavelength nanoslits of a noble metal grating, leads to giant enhancements of the magnitude of the MO effects that would normally be obtained on just the bare substrate. We show here that even more than just an enhancement, the MO effects can also undergo a sign reversal by achieving a hybridization of the different types of resonances at play in these EOT nanogratings. By tuning the geometrical profile of the grating's slits, one can engineer — for a fixed wavelength and fixed magnetization — the transverse MO Kerr effect (TMOKE) reflectivity of such a magnetoplasmonic system to be enhanced, extinguished or inversely enhanced. We have fabricated gold gratings with varying nanoslit widths on a Bi-substituted gadolinium iron garnet and experimentally confirmed such a behavior using a customized magneto-optic Mueller matrix ellipsometer. This demonstration allows new design paradigms for integrated nonreciprocal circuits and biochemical sensors with increased sensitivity and reduced footprint.

References

1. G. Armelles, A. Cebollada, A. García-Martín, and M. U. González, "Magnetoplasmonics: Combining Magnetic and Plasmonic Functionalities," Adv. Opt. Mater. **1**, 10–35 (2013).
2. M. I. Stockman, "Nanoplasmonics: past, present, and glimpse into future," Opt. Express **19**, 22029 (2011).
3. V. V. Temnov, G. Armelles, U. Woggon, D. Guzatov, A. Cebollada, A. Garcia-Martin, J.-M. Garcia-Martin, T. Thomay, A. Leitenstorfer, and R. Bratschitsch, "Active magneto-plasmonics in hybrid metal-ferromagnet structures," Nat. Photonics **4**, 107–111 (2010).
4. V. I. Belotelov, L. E. Kreilkamp, I. a. Akimov, a. N. Kalish, D. a. Bykov, S. Kasture, V. J. Yallapragada, A. Venu Gopal, a. M. Grishin, S. I. Khartsev, M. Nur-E-Alam, M. Vasiliev, L. L. Doskolovich, D. R. Yakovlev, K. Alameh, a. K. Zvezdin, and M. Bayer, "Plasmon-mediated magneto-optical transparency." Nat. Commun. **4**, 2128 (2013).
5. V. V. Temnov, "Ultrafast acousto-magneto-plasmonics," Nat. Photonics **6**, 728–736 (2012).
6. G. a. Wurtz, W. Hendren, R. Pollard, R. Atkinson, L. L. Guyader, a. Kirilyuk, T. Rasing, I. I. Smolyaninov, and a. V. Zayats, "Controlling optical transmission through magneto-plasmonic crystals with an external magnetic field," New J. Phys. **10**, 105012 (2008).
7. K. F. MacDonald, Z. L. Sámson, M. I. Stockman, and N. I. Zheludev, "Ultrafast active plasmonics," Nat. Photonics **3**, 55–58 (2009).
8. K. F. MacDonald and N. I. Zheludev, "Active plasmonics: Current status," Laser Phot. Rev. **4**, 562–567 (2010).
9. D. Jalas, A. Petrov, M. Eich, W. Freude, S. Fan, Z. Yu, R. Baets, M. Popović, A. Melloni, J. D. Joannopoulos, M. Vanwolleghem, C. R. Doerr, and H. Renner, "What is — and what is not — an optical isolator," Nat. Photonics **7**, 579–582 (2013).

10. A. Grunin, A. Zhdanov, A. Ezhov, E. Ganshina, and A. Fedyanin, "Surface-plasmon-induced enhancement of magneto-optical kerr effect in all-nickel subwavelength nanogratings," Appl. Phys. Lett. **97**, 261908 (2010).
11. V. I. Belotelov, I. A. Akimov, M. Pohl, V. A. Kotov, S. Kasture, A. S. Vengurlekar, A. V. Gopal, D. R. Yakovlev, A. K. Zvezdin, and M. Bayer, "Enhanced magneto-optical effects in magnetoplasmonic crystals." Nat. Nanotechnol. **6**, 370–6 (2011).
12. J. Y. Chin, T. Steinle, T. Wehlus, D. Dregely, T. Weiss, V. I. Belotelov, B. Stritzker, and H. Giessen, "Nonreciprocal plasmonics enables giant enhancement of thin-film Faraday rotation," Nat. Commun. **4**, 1599 (2013).
13. L. Halagacka, M. Vanwolleghem, F. Vaurette, J. Ben-Youssef, P. Gogol, N. Yam, K. Postava, B. Dagens, and J. Pištora, "Experimental demonstration of anomalous nonreciprocal optical response of 1D periodic magnetoplasmonic nanostructures," in *Proc. SPIE Integrated Optics: Devices, Materials, and Technologies XVIII,* J. E. Broquin and G. Nunzi Conti, eds. (2014), p. 89880E.
14. D. Floess, M. Hentschel, T. Weiss, H.-U. Habermeier, J. Jiao, S. G. Tikhodeev, and H. Giessen, "Plasmonic analog of electromagnetically induced absorption leads to giant thin film faraday rotation of 14," Phys. Rev. X **7**, 021048 (2017).
15. G. Ctistis, E. Papaioannou, P. Patoka, J. Gutek, P. Fumagalli, and M. Giersig, "Optical and magnetic properties of hexagonal arrays of subwavelength holes in optically thin cobalt films." Nano Lett. **9**, 1–6 (2009).
16. E. T. Papaioannou, V. Kapaklis, P. Patoka, M. Giersig, P. Fumagalli, A. Garcia-Martin, E. Ferreiro-Vila, and G. Ctistis, "Magneto-optic enhancement and magnetic properties in Fe antidot films with hexagonal symmetry," Phys. Rev. B **81**, 054424 (2010).
17. V. Bonanni, S. Bonetti, T. Pakizeh, Z. Pirzadeh, J. Chen, J. Nogués, P. Vavassori, R. Hillenbrand, J. Akerman, and A. Dmitriev, "Designer magnetoplasmonics with nickel nanoferromagnets." Nano Lett. **11**, 5333–8 (2011).
18. N. Maccaferri, A. Berger, S. Bonetti, V. Bonanni, M. Kataja, Q. H. Qin, S. van Dijken, Z. Pirzadeh, A. Dmitriev, J. Nogués, J. Å kerman, and P. Vavassori, "Tuning the Magneto-Optical Response of Nanosize Ferromagnetic Ni Disks Using the Phase of Localized Plasmons," Phys. Rev. Lett. **111**, 167401 (2013).
19. J. González-Díaz, a. García-Martín, G. Armelles, D. Navas, M. Vázquez, K. Nielsch, R. Wehrspohn, and U. Gösele, "Enhanced Magneto-Optics and Size Effects in Ferromagnetic Nanowire Arrays," Adv. Mater. **19**, 2643–2647 (2007).
20. J. B. González-Díaz, A. García-Martín, J. M. García-Martín, A. Cebollada, G. Armelles, B. Sepúlveda, Y. Alaverdyan, and M. Käll, "Plasmonic Au/Co/Au nanosandwiches with enhanced magneto-optical activity." Small (Weinheim an der Bergstrasse, Ger. **4**, 202–5 (2008).
21. G. Armelles, a. Cebollada, a. García-Martín, J. M. García-Martín, M. U. González, J. B. González-Díaz, E. Ferreiro-Vila, and J. F. Torrado, "Magnetoplasmonic nanostructures: systems supporting both plasmonic and magnetic properties," J. Opt. A: Pure Appl. Opt. **11**, 114023 (2009).
22. D. Regatos, B. Sepúlveda, D. Fariña, L. G. Carrascosa, and L. M. Lechuga, "Suitable combination of noble/ferromagnetic metal multilayers for enhanced magneto-plasmonic biosensing." Opt. Express **19**, 8336–8346 (2011).
23. G. Armelles, A. Cebollada, A. García-Martín, J. Montero-Moreno, M. Waleczek, and K. Nielsch, "Magneto-optical properties of core–shell magneto-plasmonic au–co x fe3–x o4 nanowires," Langmuir **28**, 9127–9130 (2012).
24. I. Zubritskaya, N. Maccaferri, X. Inchausti Ezeiza, P. Vavassori, and A. Dmitriev, "Magnetic control of the chiroptical plasmonic surfaces," Nano Lett. (2017).
25. G. Armelles, B. Caballero, A. Cebollada, A. Garcia-Martin, and D. Meneses-Rodríguez, "Magnetic Field Modification of Optical Magnetic Dipoles," Nano Lett. p. 150206093825004 (2015).
26. M. G. Barsukova, A. S. Shorokhov, A. I. Musorin, D. N. Neshev, Y. S. Kivshar, and A. A. Fedyanin, "Magneto-optical response enhanced by mie resonances in nanoantennas," ACS Photonics **4**, 2390–2395 (2017).
27. V. Safarov, V. Kosobukin, C. Hermann, G. Lampel, J. Peretti, and C. Marlière, "Magneto-optical Effects Enhanced by Surface Plasmons in Metallic Multilayer Films," Phys. Rev. Lett. **73**, 3584–3587 (1994).
28. T. Kaihara, T. Ando, H. Shimizu, V. Zayets, H. Saito, K. Ando, and S. Yuasa, "Enhancement of magneto-optical Kerr effect by surface plasmons in trilayer structure consisting of double-layer dielectrics and ferromagnetic metal," Opt. Express **23**, 11537 (2015).
29. C. S. Levin, C. Hofmann, T. A. Ali, A. T. Kelly, E. Morosan, P. Nordlander, K. H. Whitmire, and N. J. Halas, "Magnetic- plasmonic core- shell nanoparticles," ACS Nano **3**, 1379–1388 (2009).
30. L. Wang, C. Clavero, Z. Huba, K. J. Carroll, E. E. Carpenter, D. Gu, and R. a. Lukaszew, "Plasmonics and enhanced magneto-optics in core-shell co-ag nanoparticles." Nano Lett. **11**, 1237–40 (2011).
31. D. Meneses-Rodríguez, E. Ferreiro-Vila, P. Prieto, J. Anguita, M. U. González, J. M. García-Martín, A. Cebollada, A. García-Martín, and G. Armelles, "Probing the electromagnetic field distribution within a metallic nanodisk." Small **7**, 3317–23 (2011).
32. V. I. Belotelov, D. A. Bykov, L. L. Doskolovich, A. N. Kalish, and A. K. Zvezdin, "Extraordinary transmission and giant magneto-optical transverse Kerr effect in plasmonic nanostructured films," J. Opt. Soc. Am. B **26**, 1594 (2009).
33. L. E. Kreilkamp, V. I. Belotelov, J. Y. Chin, S. Neutzner, D. Dregely, T. Wehlus, I. A. Akimov, M. Bayer, B. Stritzker, and H. Giessen, "Waveguide-plasmon polaritons enhance transverse magneto-optical kerr effect," Phys. Rev. X **3**, 041019 (2013).
34. Štefan Višňovský, *Optics in magnetic multilayers and nanostructures* (CRC, 2006).
35. H. Takeda and S. John, "Compact optical one-way waveguide isolators for photonic-band-gap microchips," Phys. Rev. A **78**, 1–15 (2008).

36. A. B. Khanikaev, S. H. Mousavi, G. Shvets, and Y. S. Kivshar, "One-Way Extraordinary Optical Transmission and Nonreciprocal Spoof Plasmons," Phys. Rev. Lett. **105**, 126804 (2010).
37. Z. Wang and S. Fan, "Optical circulators in two-dimensional magneto-optical photonic crystals," Opt. Lett. **30**, 1989–1991 (2005).
38. N. Kono, K. Kakihara, K. Saitoh, and M. Koshiba, "Nonreciprocal microresonators for the miniaturization of optical waveguide isolators," Opt. Express **15**, 7737–7751 (2007).
39. Y. Shoji, T. Mizumoto, H. Yokoi, I.-W. Hsieh, and R. M. Osgood, "Magneto-optical isolator with silicon waveguides fabricated by direct bonding," Appl. Phys. Lett. **92**, 071117 (2008).
40. P. Dulal, A. D. Block, T. E. Gage, H. A. Haldren, S.-Y. Sung, D. C. Hutchings, and B. J. Stadler, "Optimized magneto-optical isolator designs inspired by seedlayer-free terbium iron garnets with opposite chirality," ACS Photonics **3**, 1818–1825 (2016).
41. L. Halagačka, M. Vanwolleghem, K. Postava, B. Dagens, and J. Pištora, "Coupled mode enhanced giant magnetoplasmonics transverse Kerr effect," Opt. Express **21**, 21741–21755 (2013).
42. L. Halagačka, K. Postava, M. Vanwolleghem, F. Vaurette, J. B. Youssef, B. Dagens, and J. Pištora, "Mueller matrix optical and magneto-optical characterization of bi-substituted gadolinium iron garnet for application in magnetoplasmonic structures," Opt. Mater. Express **4**, 1903–1919 (2014).
43. G. D. Aguanno, N. Mattiucci, M. J. Bloemer, D. D. Ceglia, M. A. Vincenti, and A. Alù, "Transmission resonances in plasmonic metallic gratings," J. Opt. Soc. Am. B **28**, 253–264 (2011).
44. F. J. García de Abajo, "Colloquium : Light scattering by particle and hole arrays," Rev. Mod. Phys. **79**, 1267–1290 (2007).
45. L. Halagačka, K. Postava, and J. Pištora, "Analysis and modeling of depolarization effects in mueller matrix spectroscopic ellipsometry data," Proc. Mat. Sci. **12**, 112–117 (2016).
46. J. Dionne, L. Sweatlock, H. Atwater, and a. Polman, "Plasmon slot waveguides: Towards chip-scale propagation with subwavelength-scale localization," Phys. Rev. B **73**, 1–9 (2006).
47. F. De León-Pérez, G. Brucoli, F. J. García-Vidal, and L. Martín-Moreno, "Theory on the scattering of light and surface Plasmon polaritons by arrays of holes and dimples in a metal film," New J. Phys. **10** (2008).
48. A. T. M. Anishur Rahman, P. Majewski, and K. Vasilev, "Extraordinary optical transmission: coupling of the Wood–Rayleigh anomaly and the Fabry–Perot resonance," Opt. Lett. **37**, 1742 (2012).
49. A. K. Zvezdin and A. Kotov, *Modern Magnetooptics and Magnetooptical Materials* (Institute of Physics Publishing, 1997).

1. Introduction

Magnetoplasmonics [1] — a recently coined term referring to any physical system exploiting the combined effect of a magnetic and a plasmonic functionality — is attracting a surge of interest in recent years. This research domain knows two main driving forces. On the one hand, the use of a magnetic field to add an active control, such as switching and modulation, to plasmonic-based nanophotonic circuitry [2] has been proven a compact, reliable and fast alternative [3–6] to more complex control agents such as nonlinearities [7, 8]. Secondly and more importantly, plasmonic field concentration has been exploited to enhance the unique time reversal breaking properties of magneto-optic (MO) materials [9]. In recent years numerous experimental reports have demonstrated the strong enhancement of all traditional nonreciprocal MO phenomena — complex Kerr and Faraday rotation and complex transverse Kerr phase shift — due to coupling with propagating surface plasmon polaritons or excitation of localised plasmon resonances. A wide range of magnetoplasmonic configurations has been investigated: semi-transparent dielectric magnetic iron garnet films coupled to noble metal nanogratings [6, 10–14], nanogratings of pure ferromagnetic (FM) metal thin films [15, 16], FM nanoparticles [17, 18] and nanowires [19] on dielectric substrates, hybrid ferromagnetic/noble metal sandwiches both in nanoparticle or nanowires [20–23], systems of coupled plasmonic and ferromagnetic nanoparticles [24], inverted Babinet nanohole layouts [25, 26] and propagating SPP layout [27, 28], and magnetic/plasmonic core-shell nanoparticles [29–31].

All these demonstrations share the same conceptual approach to boost the magneto-optic properties of the system: by operating closely to a high quality factor plasmonic resonance the impact of an otherwise weak MO phenomenon is sharply enhanced. A particularly convincing example of plasmonic enhanced magneto-optics is the demonstration of giant transverse MO Kerr reflectivity (TMOKE) when applying a one-dimensional plasmonic slit grating on a transparent magneto-optic iron garnet substrate (which can be possibly used as an optical waveguide) that

is magnetized in-plane and parallel to the grating's slits [32, 33]. By themselves, lossless MO materials (such as iron garnets in the near infrared region) can fundamentally not exhibit nonreciprocal TMOKE intensity effects [34, Eq. (1.138)]. However by coupling a transparent MO garnet to the Wood anomalies of a gold extraordinary transmission grating, nonreciprocal intensity reflectivities are obtained that even exceed those of strongest lossy FM metals.

In many optimized layouts for nonreciprocal circuits (such as isolators and circulators) it is inevitable to have antisymmetric magnetized regions in order to break also the spatial inversion symmetries [35, 36], to optimize the MO interaction with the symmetries of the modes at play [37, 38] or to achieve a more powerful push-pull configuration for the nonreciprocal effect [39, 40]. Gaining control over the sign of the nonreciprocity by plasmonic engineering would allow realizing such layouts without the need for complicated inverted magnetic domains and just having a uniform magnetization in the whole structure.

Differently and adding to these demonstrations of magnetoplasmonic nonreciprocity enhancement, we report here on the anomalous control of the sign of the nonreciprocal phenomena when exploiting the different resonances in a magnetoplasmonic system [41]. Apart from the obvious interest of investigating controlled tuning of resonances in magnetoplasmonic systems and their impact on the MO enhancement, there is another important motivation for controlling the sign of the nonreciprocity at play. Time reversal breaking (or thus nonreciprocity) is governed by the sense of the magnetization in the system. Up to first order, inverting the magnetization will invert the sign of the nonreciprocal phenomenon at play. Naturally, in design of the magnetoplasmonic gratings and arrays, the optical reciprocity can be tuned by controlling of the wavevector/angle of incidence [11]. We demonstrate additional degree of freedom in controlling of the magnetooptical nonreciprocity based on tuning of the coupling between resonances without changes of the electromagnetic wave properties.

2. Experimental demonstration of sign control and enhancement of magnetoplasmonic effect

2.1. Magnetoplasmonic grating design, fabrication, and characterization

To investigate magnetoplasmonic sign control and enhancement, we have designed and fabricated one-dimensional (1D) lamellar gold nanogratings on the 4 μm thick, compositionnally optimized, Bi-substituted gadolinium iron garnet (Bi:GIG),
$Gd_{1.24}Pr_{0.48}Bi_{1.01}Lu_{0.27}Fe_{4.38}Al_{0.6}O_{12}$ grown by liquid phase epitaxy (LPE) on the substituted Gadolinium Gallium Garnet (CaMg-GGG, lattice parametter a_s = 12.498 Å) substrate. Fig.1a schematically represents the studied structure. A number of square patches containing 600 periods (Λ = 500 nm) of 300 μm long and 93.7 nm thick Au stripes separated by nanoslits, have been processed by standard lift-off techniques. [42]

The first set of samples was fabricated by varying the e-beam exposure dose per written patch: the width r of the nanoslit is varied from patch to patch (see Fig. 1b). In this way we expect all developed patches have the same period and thickness of deposited gold. Therefore, the effect of the nanoslit width on the magnetoplasmonic properties of the grating is directly comparable. To complete our study in investigation of the sign control, two additional sets of patches with gold thickness of 118 nm and 134 nm were fabricated. The new fabricated sets of patches were analyzed and two patches with similar nanoslit widths were selected. Therefore, MO response of the patches which are different only in the thickness can be directly compared.

The grating's optical response have been probed by using a spectroscopic Mueller matrix ellipsometer Wooollam RC2-DI (J.A. Woollam Co.) operating in spectral range from 0.74 eV to 6.42 eV. To measure magnetooptical response of the samples, the ellipsometer was extended with in-house design computer controlled in-plane permanent magnet circuit. See Ref. [42] for more details about parametrized model of the studied plasmonic gratings and used optical optical and magnetooptical functions of materials.

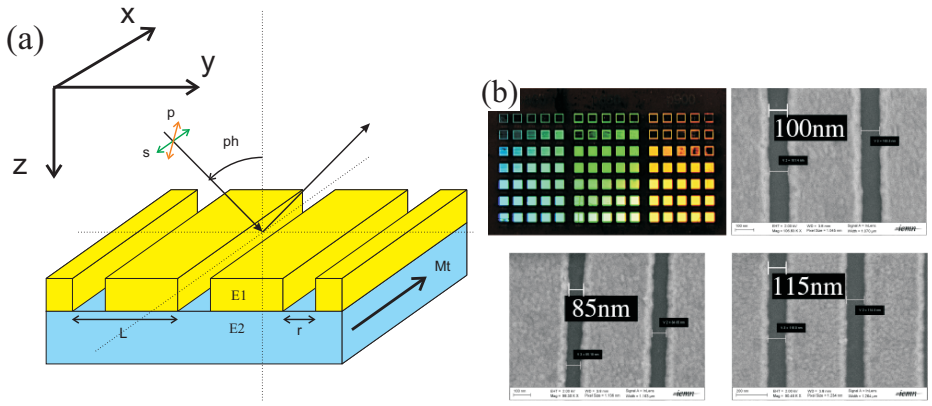

Fig. 1. (a) Definition of parameters in the model describing the magnetoplasmonic structure in planar diffraction configuration, (b) fabricated set of diffraction gratings with SEM images of developed plasmonic gratings showing good quality of the grating lamelas and observed widths of nanoslits r.

For straightforward comparison of measured and calculated optical data the ratio of reflected intensity of p- and s-polarized light, $\mathscr{R} = \frac{R_p}{R_s} = \frac{|r_p|^2}{|r_s|^2}$, is used in this paper. MO properties of the gratings are evaluated through their TMOKE reflectivity spectra $\delta\mathscr{R}$, obtained by subtracting the reflectivity spectra measured for two opposite magnetization directions ($\mathbf{M} = \pm|M|\,\mathbf{x}$), $\delta\mathscr{R} = \mathscr{R}(+\mathbf{M}) - \mathscr{R}(-\mathbf{M})$.

2.2. *Measured magnetooptical response of plasmonic nanogratings with different nanoslit width*

Fig. 2a and 2b directly compare measured MO data on 15 samples having different width of nanoslit with MO numerical simulation data. Experimental data were measured at the nominal angle of incidence of 20°. Numerical simulations were calculated for the incident angle of 20°. The systematic shift of the peak position in model proves observed trend in the experiment. Clearly at a given photon energy, for example 1.68 eV, the TMOKE response can be positive (nanoslit width r=120 nm) or negative (r=70 nm). In other words, for a given optical signal and a given magnetization the reciprocity sign is inverted by changing only the slit width.

2.3. *Measured magnetooptical response of plasmonic nanogratings with different thickness of the gold gratings and comparable slit width*

For complete analysis of the FP and SPP modes coupling here we also demonstrate tuning of TMOKE via plasmonic grating thickness. According to Eq. (2) the dispersion of the FP modes is strongly affected by the length of the resonant cavity, which is in our case presented by thickness of the gold grating h. For direct demonstration of the induced coupling, two sets of the grating samples with different thicknesses were fabricated by the same procedure of electron beam dose variation as was described above. Samples were measured and characterized with the Mueller matrix ellipsometry. By the detailed analysis of all fabricated patches we have determined thickness and nanoslits width of all samples.

The gold grating thickness of new set of samples was determined to be h = 118 nm and h = 142 nm, respectively. For direct demonstration of impact of SPP and FP modes coupling on MO response, the two patches with comparable nanoslit widths r = 148 nm and r = 137 nm were selected. Figure 3 shows detail on MO response $\delta\mathscr{R}$ observed for both mentioned samples at position of the 2nd SPP peak. In our case it is clearly visible that measured MO response (blue

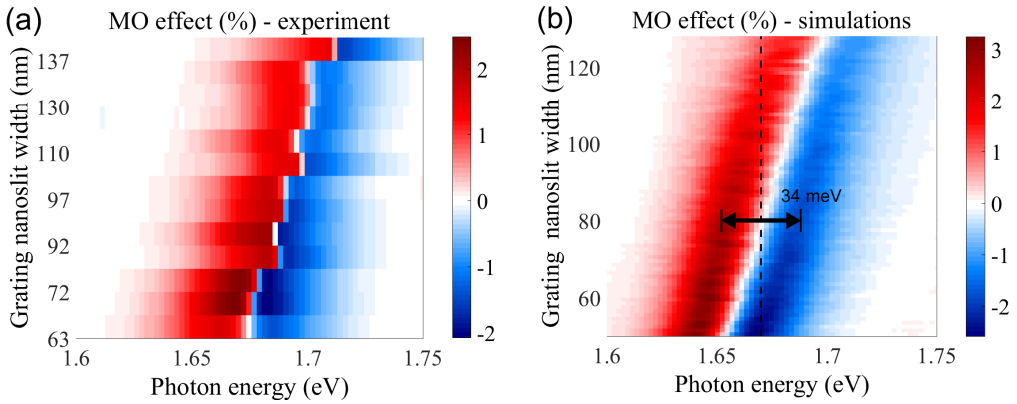

Fig. 2. Experimentally observed MO response (a) ($\delta\mathscr{R}$) measured at incident angle of 20° on 15 different patches of samples with various opening r is compared with numerical model calculated for various nanoslit width r. (b) Black dashed line at photon energy 1.67 eV highlighting the change of the MO peak sign with the grating nanoslit width r .

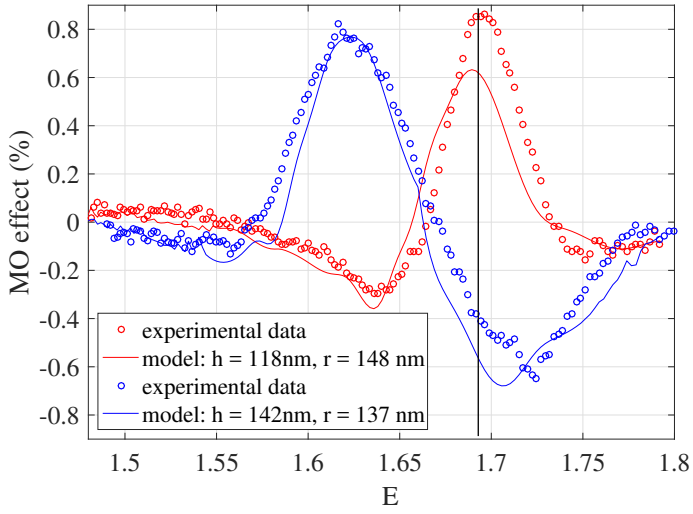

Fig. 3. Magneto-optical data measured on gratings with thickness 118 nm and 142 nm (geometry was determinend using numerical fitting procedure) are compared with model data. A significant shift of the TMOKE peak due to grating's thickness change is observed, while the nanoslit width variation is negligible. The black solid line shows spectral position on which switching of sign of the MO effect was directly experimentally observed.

and red circles) at 1.7 eV (black line in Fig. 3) is positive for the patch with thickness $h = 118$ nm and negative for the patch with grating thickness $h = 142$ nm. The MO sign inverting phenomena by the grating thickness is observed for the 2nd SPP peak, the same SPP peak as used for the switching demonstration by the grating nanoslit width. In addition in Fig. 3 calculated MO response is shown with red and blue solid lines. The MO response was calculated from model used for determination of the geometry of individual patches. Very good agreement between measured and calculated data proves validity of the used model.

In order to understand the origin of this property and to be able to control it, we have analyzed

more deeply the reflectivity spectrum of such samples, firstly without magnetization. In the next step, the influence of the magnetooptical activity is introduced in model of the SPPs EOT resonances.

3. Operational principle of resonant modes in magnetoplasmonic grating

Optical and magnetooptical activity of samples were studied in planar diffraction configuration. With the plane of incidence perpendicular to the grating direction, the ellipsometric specular intensity ratio $\frac{R_p}{R_s}$ obtained in such measurements will contain the signatures of the surface plasmon polariton (SPP) anomalies of the EOT nanoslit grating. In particular, due to the strong subwavelength nature of the slits the structure has a smooth and overall strong spectral s-reflectivity R_s, while the p-reflectivity R_p exhibits sharp peaks at the spectral position of the diffractively folded surface plasmon polaritons, $k_{\mathrm{SPP}}(E_{\mathrm{ph}}) = \frac{E_{\mathrm{ph}}}{hc}\sqrt{\frac{\epsilon_{\mathrm{Au}}\epsilon_{\mathrm{Bi:GIG}}}{\epsilon_{\mathrm{Au}}+\epsilon_{\mathrm{Bi:GIG}}}} + m\frac{2\pi}{\Lambda}$ $(m = \pm 1, \pm 2, \dots)$.

The SPP EOT transmission maxima occur slightly blueshifted with respect to these peaks. [43, 44]. Due to the overall smooth R_s, the sharp Fano-like minima in $\frac{R_p}{R_s}$ therefore correspond to the detection of the Wood plasmon transmission anomalies of the gold grating.

The measured ellipsometric spectrum for an incidence angle of $\varphi = 20°$ on a 100 nm thick gold grating formed by a periodic arrangement of strong sub-λ slits ($r = 63$ nm and $\Lambda = 500$ nm) show systematic shift of the reflectivity $\mathscr{R}$ dip from 1.68 eV to 1.7 eV for the nanoslit width change from 63 nm to 130 nm (Fig. 4b). As the inset of the Fig. 4a shows, the observed Fano resonances indeed appear close to the crossings of the 20°−light line (solid black) with the theoretically calculated dispersion of the folded SPPs on a flat Au/garnet interface (solid blue). In addition, experimental data were measure for configuration in witch SPPs modes are separates in spectrum. Therefore, the interaction between different SPPs in minimal and their interaction with FP resonant modes can be studied directly.

Interestingly, when zooming in on the measured reflectivity spectra close the $+2^{\mathrm{nd}}$ order garnet/Au SPP, a pronounced redshift of the extraordinary reflection resonance is observed for gratings with decreasing width of nanoslit (Fig. 4b). The Rigorous Coupled Wave Algorithm (RCWA) was used for optical modeling of the plasmonic grating. The widths of nanoslits have been obtained by a single global least-squares fit of model to measured ellipsometric data. The measured spectra for 15 patches with different nanoslit have been processed in a single step on the same garnet substrate. The fitting procedure accounted for the presence of a top roughness layer on the fabricated gold gratings and for depolarization effects due to an angular spread of the incident Gaussian beam [45]. It must be noted that the fitted nanoslit widths r follow the trend of the values estimated by SEM observation r_{SEM} (as shown on Fig.1b).

3.1. Optical observation of the effect of coupling between SPP and FP resonances

In the following we will explain the phenomena of tuning the plasmon resonances and MO sign conversion by a simple model of coupling SPP and Fabry-Pérot (FP) modes. In a first approximation, this resonance shift as a function of nanoslit width r cannot be explained by the diffractive folding of the Au/garnet SPP dispersion, as this latter is only parametrically dependent on the grating's period Λ, the incidence angle φ, and the Au and Bi:GIG permittivity, $\varepsilon_{\mathrm{Au}}$ and $\varepsilon_{\mathrm{Bi:GIG}}$. In previous theoretical work we demonstrated how variations of the grating's geometry (in particular its thickness h) causes an anticrossing interaction of the diffractively coupled SPP resonances and the FP slit resonances undergone by the guided TM mode in the subwavelength metal/insulator/metal slit. [46] Increasing thickness leads to an increasing geometric phase of the fundamental TM slit mode, $\frac{\omega}{c} n_{\mathrm{eff,TM_0}} h$, thereby redshifting the FP EOT resonances. Due to anticrossing the SPP reflection anomalies will therefore eventually also redshift with the grating thickness h.

In a first approximation the spectral position of the grating's resonances as a function of

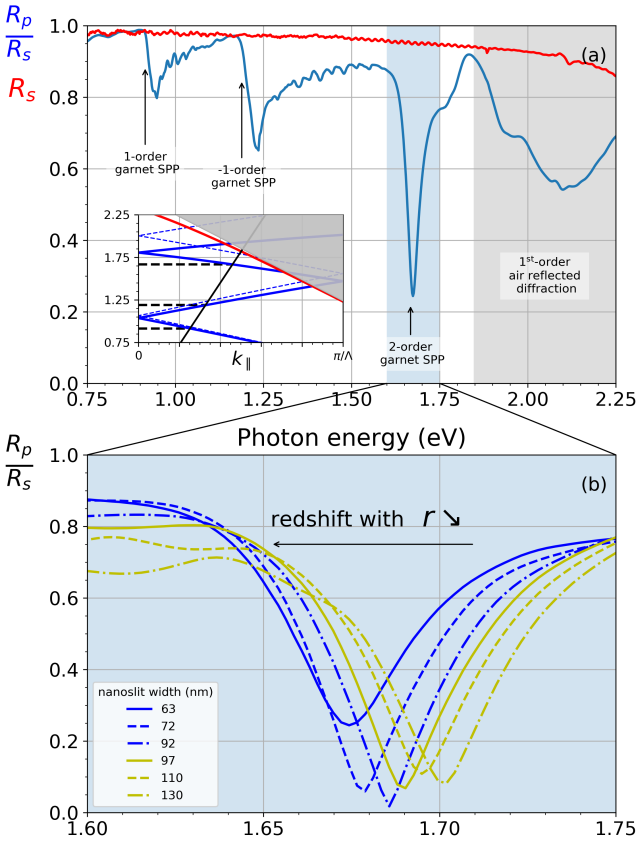

Fig. 4. Spectra of relative reflectance $\mathscr{R} = R_p/R_s$ measured for the angle of incidence $\varphi = 20^\circ$, grating nanoslit width $r = 63$ nm, and the grating thickness $h = 100$ nm. In subplot (a) the full spectra is presented with marked position of the 1st and 2nd garnet SPP peaks. The inserted detail of light-cone includes dispersion curves of the predicted SPP (solid blue) crossing the 20° - light line (solid black). The area for air SPP is marked as red line. Subplot (b) detail red/shift of the +2nd garnet SPP peak measured for increasing width of the nanoslit r.

its geometrical parameters ($h, r,$ andΛ), can be obtained by solving the following dispersion equations for the photon energy E:

$$\text{SPP}: \pm k_{\text{SPP}}(E) \mp m_1 \frac{2\pi}{\Lambda} = \frac{E}{\hbar c}\sqrt{\varepsilon_i(E)}\sin(\varphi_{\text{inc}}), \quad m_1 \in \mathbb{N} \text{and} i \in \{\text{air}, \text{Bi}:\text{GIG}\}, \tag{1}$$

$$\left[k_{\text{SP}}(E) = \frac{E}{\hbar c}\sqrt{\frac{\varepsilon_{\text{Au}}(E)\varepsilon_i(E)}{\varepsilon_{\text{Au}}(E)+\varepsilon_i(E)}}\right]$$

$$\text{FP}: \frac{E}{\hbar c} 2 n_{\text{eff,FP}}(E) h + \phi_{r_{\text{air}}}(E) + \phi_{r_{\text{Bi:GIG}}}(E) = 2 m_2 \pi, \quad m_2 \in \mathbb{N}_0. \tag{2}$$

Here $n_{\text{eff,FP}}$ is the effective index of the fundamental TM mode of the Au/air/Au plasmonic

waveguide formed by the nanoslit and obtained by solving [46]

$$\tanh\left(\frac{rE}{2\hbar c}\sqrt{n_{\mathrm{eff,FP}}^2-1}\right)=-\frac{\sqrt{n_{\mathrm{eff,FP}}^2-\varepsilon_{\mathrm{Au}}(E)}}{\varepsilon_{\mathrm{Au}}(E)\sqrt{n_{\mathrm{eff,FP}}^2-1}}. \tag{3}$$

The reflection phase shifts, ϕ_{r_i}, at both ends of the slit cavity can in first approximation be those of normal plane wave incidence, $r_i = |r_i|\exp(i\phi_{r_i}) = \frac{n_{\mathrm{eff,FP}}-\sqrt{\varepsilon_i}}{n_{\mathrm{eff,FP}}+\sqrt{\varepsilon_i}}$. Beside the SPP resonances depend only on Λ and φ_{inc}, and are independent of the grating's geometrical parameters governing the FP spectral location, h and r, as seen from Eqs. 1-3. Varying therefore only, for instance, the nanoslit width r at fixed incidence angle and grating periodicity may lead to SPP-FP resonance coupling.

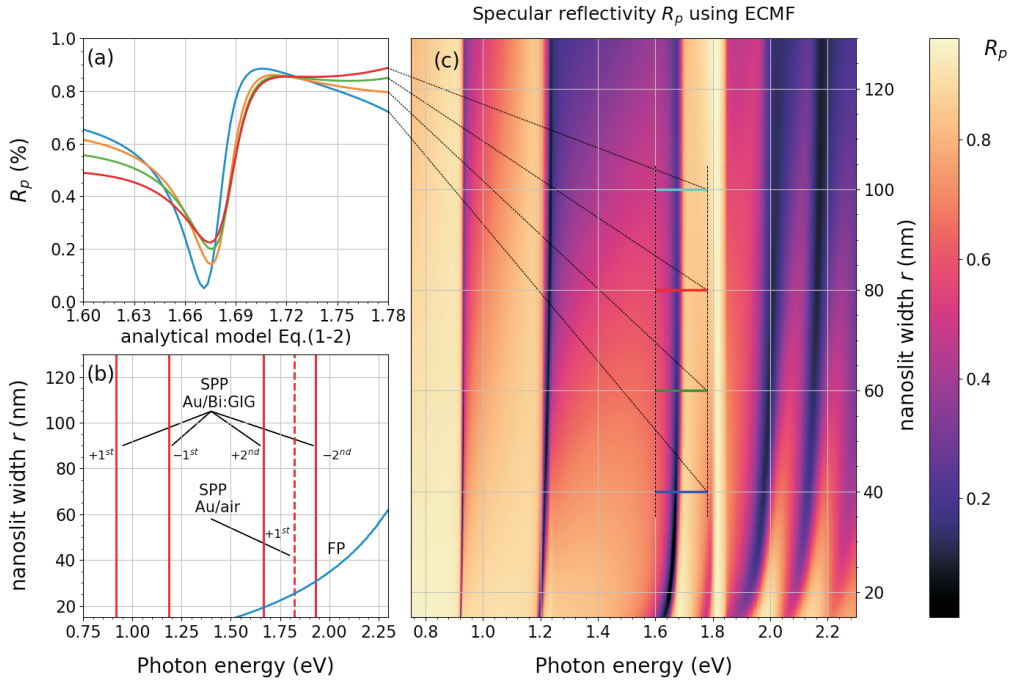

Fig. 5. Analysis of coupling between FP and SPP modes base on variation of the grating air-gap width r. Subplot (a) shows red-shift of coupled SPP/FP mode at cross-cuts for air-gap width $r = 40, 60, 80$, and 100 nm. Subplot (b) shows positions of the SPP modes without geometrical dispersion and dispersive FP mode (calculated from Eq. (1, 2)). Subplot (c) shows dispersion map of SPPs and FP modes calculated using extended coupled-mode formalism.

Fig. 5b illustrates this for the case of $\varphi_{\mathrm{inc}} = 20°$ and $h = 100$ nm, corresponding to the experimental conditions of Fig. 2a. From Eq. (3) one can deduce how the decreasing slit width r will cause an increase of $n_{\mathrm{eff,FP}}$, which in turn by Eq. (2) will redshift the FP resonance. The FP slit resonance (blue) is seen to cross the 2^{nd}−order Au/garnet SPPs (red) for nanoslits widths between 20 and 40 nm. Due to anticrossing mode coupling the otherwise fixed energy of the 2^{nd}−order SPPs will be perturbed even for slit widths values beyond this range. This is demonstrated in Fig. 5c where we have numerically calculated the specular reflectivity spectrum

R_p for a range of slit widths (at $\varphi_{\text{inc}} = 20°$) using an extended coupled-mode formalism [(ECMF), see Ref. [47]]. The reflection minima corresponding to the different mentioned grating resonances can be distinguished, but more importantly their coupling and anticrossing in the region predicted in Fig. 5b is convincingly observed. Fig. 5a zooms in on the redshift of the $2^{\text{nd}}-$order Au/garnet SPP. The experimentally observed redshift of the plasmonic grating reflection anomaly can therefore be correctly attributed to a coupling between FP and SPP resonances. This experimental observation confirms for the first time the previously suggested theoretical possibility of tuning the strength of the EOT effects only by tuning of one geometrical parameter [41, 48].

3.2. Study of magnetooptical perturbation of the SPPs EOT modes

Turning our attention to the magnetic character of the garnet substrate of the studied plasmonic nanograting, we explore the impact of the observed coupling between the grating's resonances on the magneto-optic activity of the system. In MO materials the presence of a magnetization creates antisymmetric off-diagonal components in the permittivity tensor, $\overleftrightarrow{\varepsilon} = \begin{pmatrix} \varepsilon & +ig_z & -ig_y \\ -ig_z & \varepsilon & +ig_x \\ +ig_y & -ig_x & \varepsilon \end{pmatrix}$, where in first order the gyration vector $\mathbf{g} = g\mathbf{1}_M$ is parallel to the magnetization and its magnitude is linearly proportional to that of $\mathbf{M}$, $g \sim |\mathbf{M}|$. For lossless MO media $\overleftrightarrow{\varepsilon}$ must be hermitian, so that both ε and g must be real. In the most general case this gives rise to a nonreciprocal polarization change of a polarized beam [49] when reflected from a surface of a MO layer. The fundamental process induced by the magnetization is the Lorentz force on carriers. Therefore, in a unique configuration of a magnetization perfectly perpendicular to the incidence plane, the s-wave having its E-field perfectly parallel to the magnetization, will not undergo any MO effect. In this so-called transverse configuration only the p-polarization will undergo a nonreciprocal correction. The ensuing transverse MO Kerr effect leads to a nonreciprocal first-order correction on the Fresnel reflection coefficient, $r_p = r_p^0(1 + ig\delta r_p)$, where r_p^0 is the isotropic conventional reciprocal Fresnel coefficient (for $\mathbf{M} = 0$) and the small effect correction $\delta r_p = \frac{r_p^0 g k_y}{2\varepsilon_{\text{MO}} k_{z,\text{MO}}}$. On a lossless MO material and below its critical incidence angle, TMOKE is then solely a reflection phase shift since $\text{Im}(g\delta r_p) = 0$, and the power reflectivity R_p remains perfectly reciprocal, $\Delta R_p = |r_p(\mathbf{M})|^2 - |r_p(-\mathbf{M})|^2 = 0$. Nonreciprocal power reflectivity can only be realized on absorbing media. However on bare lossy ferromagnetic metals such as Co or Fe, ΔR_p doesn't exceed 10^{-3}. [49]

On the other hand, TMOKE power nonreciprocity on a lossless MO garnet can be obtained by cladding it with a plasmonic grating. [32]. The gold/garnet SPP dispersion gets a small nonreciprocal correction due to the nonreciprocal phase shift by the transverse MO garnet substrate. In combination with the sharp reflection resonances of the grating's FP, this leads to a huge enhancement. [41]

Including the effect of the gyrotropy in the boundary conditions at the interface between gold and a transversely magnetized garnet, leads to the following nonreciprocal dispersion equation for the surface magnetoplasmon polaritons:

$$\varepsilon_{\text{Au}}(\varepsilon_{\text{Bi:GIG}} - n_{\text{eff,SPP}}^2) + \varepsilon_{\text{Bi:GIG}}\sqrt{\varepsilon_{\text{Au}} - n_{\text{eff,SPP}}^2}\sqrt{\varepsilon_{\text{Bi:GIG}} - n_{\text{eff,SPP}}^2 - \frac{g^2}{\varepsilon_{\text{Bi:GIG}}}} = ign_{\text{eff,SPP}}\sqrt{\varepsilon_{\text{Au}} - n_{\text{eff,SPP}}^2} \qquad \text{where} n_{\text{eff,SPP}} = \frac{k_y}{k_0} \quad (4)$$

The gyrotropy clearly breaks the inversion symmetry $n_{\text{eff,SPP}} \rightarrow -n_{\text{eff,SPP}}$. Linearizing this equation with respect to g — for the considered garnet [42] in the near infrared $g \approx 0.003$

(g = 0.0096 @ 1.67 eV) — and solving to first order of g:

$$n_{\mathrm{eff,SPP}} = \pm\sqrt{\frac{\varepsilon_{\mathrm{Au}}\varepsilon_{\mathrm{Bi:GIG}}}{\varepsilon_{\mathrm{Au}}+\varepsilon_{\mathrm{Bi:GIG}}}} + \frac{ig\varepsilon_{\mathrm{Au}}^2}{\left(\varepsilon_{\mathrm{Au}}^2-\varepsilon_{\mathrm{Bi:GIG}}^2\right)\sqrt{\varepsilon_{\mathrm{Au}}+\varepsilon_{\mathrm{Bi:GIG}}}}. \tag{5}$$

Similarly with non-MO configuration described by Eqs. (1-3) FP-SPP coupling occurs. The dependence of the imaginary part of $n_{\mathrm{eff,SPP}}$ with g induce non-reciprocal response of coupled FP-SPP modes. The model of MO SPP describes spectral shift of the SPP mode by MO effect by a perturbation linearly dependent on gyrotropy g. It could thus be used to predict the effect and thus to design devices based on non-reciprocal reflection or transmission with locally inverted sign. In Fig. 2b this $n_{\mathrm{eff,SPP}}$ dependence introduces spectral shift of typically $\approx$ 30 meV whatever the slit.

4. Conclusion

In this paper we have demonstrated unique approach for fine local tuning and switching of the magnetooptical effect in 1D periodic plasmonic gratings. By tuning geometrical parameters of the grating, the non-reciprocal reflectivity not only can be enhanced but also tuned in terms of sign and magnitude. The MO tuning was demonstrated experimentally and numerically for two cases: variation of the grating nanoslit width r and variation of the grating thickness h. We have proved correctness of our models used for determination of individual gratings geometry by direct comparison of measured and calculated MO response. We have also demonstrated how these significant effects can be correctly modeled with a linear analytic approach, giving easy design tool. This offers possibility of additional enhancement thanks to push-pull configuration by playing on technologically realistic combination of grating of the same thickness and different slits for advanced circuits including non-reciprocal functions.

Acknowledgment

This work has been partially supported by the french RENATECH network. The authors gratefully acknowledge the support by the Grant Agency of the Czech Republic (Project 18-22102S). CZ.02.1.01/0.0/0.0./16_013/0001791, and IT4Innovations National Supercomputing Center – LM2015070.